

Electron beam induced annealing of ion-irradiation damage in zircon

NKFIH OTKA 116183 Postdoctoral research grant

Final Report

1. Introduction: Scope and significance

The radiation damage in actinide-containing solids is a product of distributed-source self-irradiation of energetic particles. Most of the damage comes from the alpha decay of U and Th due to its highest probability among radioactive decay processes. The damage caused by alpha decay is stored in zircon through geologic times at reduced temperatures and in the lack of aggressive chemical reagents. Natural zircon therefore may be an excellent material, from crystalline through various degrees of damage to completely amorphous, for the study of the effects of self-irradiation accumulated on geologic time scales (up to billions of years).

The goal of this proposal was to gain insight into the real structure of radiation-damaged zircon and to understand better defect distributions and related spectroscopic phenomena. The idea came from an earlier experimental observation, namely, that low-energy (15–20 keV) electron beams are able to cause spectroscopically observable changes in the degree of crystalline order in zircon (Nasdala et al., 2003). The project proposed a systematic evaluation of the annealing effect of electron beams in zircon. The scope of the research project included partly an assessment of electron-induced annealing in bulk, naturally self-irradiated zircon. This part of the project is directly relevant to routine analytical conditions in zircon geochemistry and dating techniques while exploring an annealing mechanism that is in slight contrast to thermal annealing. A deeper understanding of annealing processes may lead to an improved image of the damaged state as well.

Some of the complexity presented by self-irradiation was planned to be tackled using experimentally produced samples in which either only heavy-ion irradiation (as a model for alpha recoil damage) or only light-ion irradiation (as a model for damage induced by alpha particles) was present. The plan was to evaluate the electron-induced annealing effects primarily through spectroscopic analysis, using a method that probes short, medium and long-range order (Raman spectroscopy of the zircon lattice), and another method sensitive to first-order neighbours (photoluminescence emission spectroscopy of rare earth element centres). These methods were chosen to gain insights on the transition from crystalline to (partially) amorphous matter, where the transition is driven by the damage caused by high-energy ionic radiation.

Naturally, there are many more questions to answer regarding the real structure of radiation-damaged materials and related phenomena, therefore, the scope of the project was partly shifted to involve an investigation of phonon dispersion properties, as well as of a descriptive, plausible model of the distribution, spacing and connectivity of recoil damage clusters. Phonon dispersion properties are applicable to the prediction of the behaviour of phonon frequencies (e.g. Raman shifts) and band widths in domains of very small sizes (typically in the few 10s of nanometres range), restricted by defects, dislocations or domain boundaries in dielectrics. Radiation-damaged zircon exhibits a trend in the evolution of Raman bands with increasing irradiation dose that is very similar to due to so-called phonon confinement (small contiguous crystal lattice dimensions relaxing phonon scattering selection rules; see e.g. Osswald et al., 2009). To date, however, there is no clear way to separate strain-related spectroscopic effects from those caused by phonon confinement, both of which may cause some broadening and shifting of Raman bands (Vácz & Nasdala, 2016). A comparison of the dimensions of undamaged domains as a function of irradiation dose (a complementary information from studying recoil cluster distribution) with verified phonon

dispersion properties was planned to provide useful clarification, applicable to the interpretation of spectroscopic data.

2. Materials and methods

The sample set for the study on the electron irradiation of bulk zircon samples consisted of small, approx. mm-sized, fragments of well-characterised, gem-quality zircon samples from Sri Lanka (Nasdala et al., 2004) and a synthetic, undoped ZrSiO_4 crystal for reference. The five gem zircon samples were carefully selected to span a large range from slight to heavy self-irradiation damage. Their calculated accumulated dose levels ranged from low to high (ca. $0.5 \cdot 10^{18} \alpha/\text{g}$ to ca. $2.5 \cdot 10^{18} \alpha/\text{g}$ dose), and the dose steps between them were approximately equal. These samples were unoriented, except the synthetic crystal, and were embedded and polished as would be a general-purpose sample for electron probe microanalysis (EPMA, electron microprobe). These samples were coated with a thin gold layer to avoid sample charging under the electron beam. Locating the electron irradiation spots in subsequent optical measurements were made possible by FIB-milled guide marks on sample surfaces.

In the follow-up part of this project, the original plans aimed at using synthetic, REE-doped zircon materials to be subjected to artificial ion irradiations. The actual experimental planning made it clear that it would be unmanageable, in terms of sample preparation time/effort as well as of funding, to run separate lines of heavy- and light-ion irradiations, including back-up sample sets to account for accidents and failures. The number of samples was effectively reduced by the decision that a naturally “co-doped” zircon sample would be used that is “young” (<1 million years) in geological terms, and in which the concentration of non-formula elements is particularly low. Therefore, already in its natural state, no deviation from crystallinity can be shown using Raman spectroscopy. The sample of choice was a zircon sample from Ratanakiri, Cambodia, which is famous for its blue colour acquired through heat treatment (Zeug et al., 2018). A heat-treated (i.e., having practically zero damage), large, oriented single-crystal zircon, containing trace amounts of Nd^{3+} and Dy^{3+} , was used for the preparation of the micro-lamellae. The samples were kindly made available by Prof. Lutz Nasdala (University of Vienna).

The micro-lamellae were cut using a dual-beam focussed ion beam/scanning electron microscope (FIB-SEM) instrument following manufacturer recommendations. The cut lamellae of approx. $15 \times 20 \times 1.5 \mu\text{m}$ dimensions were fixed to lift-out grids using a micro-manipulator and Pt deposition and given a low ion energy final polish (Chanmuang et al., 2016). For all experiments, two sets of lamellae were dedicated as any sample loss would cause a serious setback. No conductive coat was applied to these samples because test measurements revealed that any type of coating renders optical measurements unreliable. For the light-ion irradiation experiment, five lamellae comprised one sample set to allow for a range of ion fluences. The He-ion irradiations were planned and carried out in the 6 MV tandetron accelerator at the Helmholtz-Zentrum Dresden-Rossendorf, Germany, spanning about two orders of magnitude ($2.5 \cdot 10^{15}$ to $1 \cdot 10^{17}$ He ions/cm²).

The electron irradiations of bulk samples were done on an electron probe micro-analyser (JEOL JXA-8600 Superprobe, Faculty of Earth Science and Engineering, University of Miskolc). FIB-cut and ion-irradiated lamellae were first electron irradiated in an SEM (Thermo Scientific SCIOS 2) and later in an e-beam writer (RAITH 150 E-BEAM, both at the Institute of Technical Physics and Materials Science, Centre of Energy Research, Budapest).

Particle irradiations were augmented, in the planning and evaluation phases, by Monte Carlo simulation techniques. The stopping of helium and gold ions were modelled in SRIM2013, while electron trajectories were simulated using Casino 2.

Raman spectroscopic and photoluminescence (PL) measurements were done on high-resolution, dispersive Raman spectrometers (HORIBA LabRAM HR800 and LabRAM EVO in the Raman laboratories of the Faculty of Science, Eötvös Loránd University, Budapest and the Institute of Mineralogy and Crystallography, University of Vienna, respectively) with red (He-Ne, 632.8 nm for Raman), green (Nd-YAG, 532 nm for Nd³⁺ PL) and blue (Nd-YAG, 473 nm for Dy³⁺ PL) excitation lasers. When necessary, the deconvolution of instrumental from measured band profiles was done according to Váczi (2014).

The geometric modelling of damage distribution is a unique task for which no publicly available solutions are available. Therefore, modelling was done using a custom-made computer code, written using the Lazarus development environment in Pascal by Lajos Tóth, with scalable parameters for PC.

3. The significance of applied analytical methods

This section contains a summary of the reasons behind the selection of methods for sample analysis and modelling. The information presented here shows how the interpretation of results may aid in the progress towards research goals. This is an actual outcome of the project as the involvement in both experimental and theoretical aspects helped greatly to critically assess the capability of methods as well as the results attained. Note that some methods are included here that have no presentable results in this report but a lot of research effort went into their in-depth understanding and applicability.

3.1. Raman spectroscopy

Raman spectroscopy probes vibrational transitions through the inelastic scattering of ultraviolet–visible–near infrared (UV–vis–NIR) photons. The interaction happens on transitions between vibrational energy levels of coupled oscillators, such as molecules, chemically bound clusters in glasses or crystal lattices. Lattices are particularly important and interesting as vibrations in them take the form of collective oscillations that are synchronised across the whole lattice. Effectively this means that translational symmetry also acts on the collective vibrational motion and, in an ideal crystal, the oscillations occur as plane waves across the entire lattice. The interaction, that is, the vibrational excitation occurs in a quantised form, the magnitude of which is scaled by the oscillation frequency of the excited vibrational mode. This quantum is called a phonon. A vibrational excitation in a defect-free lattice allows an extended phonon lifetime or phonon (mean) free path. Both of these descriptive terms stem from a view of phonon propagation through the lattice. In a crystalline material, therefore, Raman scattering is a probe of long-range order. However, phonon propagation in dielectrics is typically impeded on deviations from translational symmetry such as defects (including chemical substitutions), dislocations, domain or grain boundaries etc. The reduction of phonon lifetime or mean free path can be described physically as a relaxation of the $k = 0$ wavevector selection rule (in other words, as a deviation from the so-called long-wavelength limit), and scattering away from the Brillouin zone centre becomes possible. This may appear as a change in the vibrational transition energy; the effect gives rise to the so-called phonon dispersion curves (the dependence of the transition energy on the wavevector) of any given mode of vibration. Phonon confinement is the limiting effect of grain boundaries typical for nanomaterials, which is probed very effectively by Raman spectroscopy. Since displacements from lattice sites influence the vibrational frequencies, Raman spectroscopy is also sensitive to strain effects in crystals (and glasses).

More classically, Raman spectroscopy is sensitive to strain through its influence on bond lengths and, hence, force constants and frequencies (e.g. Sheremetyeva et al., 2018). Radiation-damaged

materials are affected by macroscopic to submicroscopic inhomogeneous strain fields due to the mismatch of the ordered and the radiation-amorphised volumes. Unfortunately, the strain magnitude and distribution in such materials is unknown, therefore currently it is not possible to distinguish strain and other factors influencing spectroscopic measurements. However, the empirically established damage accumulation trend for self-irradiation in zircon (e.g. Nasdala et al. 2004) has been, and will be, used to assess the damage state of zircon samples. The Raman spectroscopy of radiation damage in zircon (regarding both accumulation and annealing) is rather extensive, therefore the literature is also an important source of data and inspiration.

3.2. Photoluminescence spectroscopy

Luminescence is the emission of photons following an electronic excitation; in photoluminescence (PL) the excitation energy is typically a UV–visible photon. The emitted photon energy (wavelength) is characteristic to the electronic structure of the emitter. However, some factors exert an influence on the electronic levels: valence, bonding and coordination (including its symmetry) may modify electronic transitions and luminescence emission. This is especially interesting in the case of certain lanthanide ions (e.g., Dy^{3+} , Nd^{3+}) because of their peculiar arrangement of the electronic energy levels. Without excessive detail, the f – f electronic transitions occur between electron levels that are weakly shielded from external electric fields. For this reason, the degeneracy of emitter and/or acceptor levels of such ions in coordinated compounds may be lifted. In a crystal lattice, the crystal field at the specific site (electric field of the symmetry-bound first neighbours) is very well known to cause such splitting of energy levels. Thus, certain rare earth element (REE) ions, such as Nd^{3+} , in a crystal exhibit a complex luminescence emission spectrum in which the properties (coordination number, bond lengths, symmetry etc.) of the first coordination sphere are reflected. This is the reason why luminescence emission may be interpreted as a probe of the short-range order in the condensed phase. This property was the major reason why REE PL spectroscopy was originally planned to evaluate defect density and annealing in zircon. Another, perhaps self-explanatory, motive was that laser-induced PL spectroscopy could also be investigated using the same type of instrument as the one used for Raman spectroscopy.

It is safe to say that natural zircon does not occur without varying levels of chemical substitutions. Most substitutions happen at the $\text{Zr}^{[8]}$ ($4a$) site. Hafnium is the most abundant substituting element but perhaps more important are uranium and thorium for a scientific (radiometric dating) and technical (radioactive waste storage) viewpoint. Trivalent rare-earth elements are also ubiquitous and compatible with the zircon lattice (Finch & Hanchar, 2003). In summary, REE^{3+} PL appeared as a promising tool to observe short-range order-disorder phenomena caused by particle irradiations in zircon. Although the literature of luminescence spectroscopy of zircon is not as rich as in the topic of Raman spectroscopy, basic to advanced observations and ideas can nevertheless be integrated from published sources (e.g. Lenz et al., 2019).

3.3. Particle irradiations

An intrinsic property of self-irradiation is the overlap of heavy-ion (recoil) damage and damage caused by the alpha particle (He^{2+}). An intriguing question is, of which only assumptions exist, the state of the volume not amorphised by recoil chains. This volume, contiguous (percolating in the sense of Salje et al., 1999) until relatively high doses, is variably assumed to be crystalline, crystalline with defects (Váczi, 2016), crystalline with strain etc. The source of scattered defects, if any, is generally assumed to be the damage introduced by the alpha particles emitted in alpha decay events. The motive for the second part of this project was to separate the effect of alpha particles from that of recoil ions through artificial ion irradiations (using either heavy or light ions) in particle

accelerators. The accumulation and subsequent annealing of damage, induced by light and heavy ions, was expected to provide new knowledge about defect mobility, the recovery of order etc. The heavy ions were planned to model alpha recoil, i.e. ions of large mass and moderate kinetic energy. These ions cause localised, heavy damage on the length scale of a few tens nanometres through direct impact damage (Ríos et al., 2000). In contrast, the stopping range of alpha particles in zircon is much longer (up to ca. 32 μm for 8.8 MeV He ions) and most of the energy transfer occurs in the form of electronic interactions, and collisions only occur at small kinetic energies (Vácz, 2016 and references therein). The damage created is generally assumed to differ from heavy-ion damage (“pearls on a string”), with a slightly elevated damage density only at the far end of the trajectories (Nasdala et al., 2011; Smye et al., 2014). Self-irradiation from a distributed source (i.e., chemical substitution by U, Th, Pu) causes an overlap of these different types of damage, making interpretations more complicated.

Due to concerns of artefacts arising from a mismatch of interaction volumes (ion stopping range vs. optical analysis) and the predictable build-up of strain due to swelling (Nasdala et al., 2010), the targets for ion irradiations were not bulk crystals. To circumvent the artefacts, the adjustment of experimental details was necessary: (1) I adopted the idea to use micro-lamellae prepared using a focussed Ga ion beam (Chanmuang et al., 2016); (2) the depth range damaged by the stopping of ions had to be extended to the full thickness of the lamellae, by planning multi-energy irradiations for both light-ion (He^{2+}) and heavy-ion (Au^+) experiments (see Nasdala et al., 2017; for details see Nasdala et al., 2018).

Electron-induced annealing was planned in the form delivering a stationary, low electron energy (20 keV), focussed electron beam into selected sample spots. The resulting micro-areas of electron-induced annealing through enhanced defect mobility were expected to be in contrast with their non-irradiated surroundings. After establishing that the annealing effect depends on the electron dose in a systematic study on a set natural zircon samples (Vácz & Nasdala, 2017), a single, large electron dose was planned in the artificially damaged samples. An obvious choice of instrument for electron treatment in this study was the electron probe micro-analyser (EPMA) as it is designed to produce a very stable electron beam with a regulated beam current for extended times for X-ray analytical purposes. Scanning electron microscopes are designed especially for high-resolution imaging, but well-maintained, modern instruments can also produce stable beams with high current. However, as problems arose presumed to be caused by a too high electron flux into FIB-cut lamellae, an electron beam lithography system (e-beam writer) of reduced beam current was also employed. The most stable and accurate of the three types of instruments is the e-beam writer, which, essentially, is also a special-purpose electron microscope without chemical analysis capabilities, though stability comes at an expense of some lack of analytical flexibility and, for my purposes, a greatly extended instrument time compared to a general-purpose instrument.

3.4. Geometric modelling

The “layout” of damaged and undamaged volume, that is, the distribution of (recoil) damage, as well as the shape, size and distribution of remaining crystalline portions in self-irradiated zircon is an issue that has been present in the literature for decades. Interpretations are based on indirect evidence such as empirical data (Ríos et al., 2000; Farnan & Salje, 2001), more direct information from simulations (e.g. Trachenko et al., 2001) and insights from other fields of science. The most successful description of the process of the accumulation of self-irradiation damage is the percolation transition (Salje et al. 1999), which provides a framework to integrate theoretical and experimental evidence from zircon studies as well as percolation theory.

The actual observation of the distribution of a statistically relevant number of recoil clusters is not possible due to scaling issues: there is no single method that could provide graphic (imaging) or indirect evidence on sizes, distributions, defect densities etc. of both crystalline and recoil-impacted volumes. One either images or simulates a single (or a few at most) recoils or can use an experimental result from the bulk. To bridge the gap, a geometric model was developed by Ketcham and co-authors (Ketcham et al., 2013). The model uses a strongly simplified representation of recoil damage (“capsules”, i.e., tubes with hemispherical caps on both ends), in randomly distributed and oriented recoil chains scaled to natural recoil kinetic energies to mimic an informed picture of natural self-irradiation. Their results, while conforming very well to the concept of percolation, predicted very different dose levels for specific points of interest (first percolation, onset of massive connectivity, undamaged volume dimensions etc.) in the percolation transition compared to those derived from experimental observations (Salje et al. 1999; Ketcham et al., 2013). However, a careful assessment identified an essential flaw in the published model: the input parameter used to scale the “capsule” sizes was an incorrect choice. In short, the amorphous fraction per recoil event created in the published model is about twice of a realistic value (this is discussed in some detail in the paper Váczi & Nasdala, 2017). The disparity means that at any number of recoil chains, the amorphous fraction introduced to the model is approximately double of the expected, experimentally supported amount (Fig. 1). These arguments warranted a recalculation of the Ketcham et al. (2013) geometrical connectivity model, as it is intuitively unpredictable how “bulk” connectivity and damage distribution would scale if the capsule sizes (lengths) were shortened by the appropriate amount.

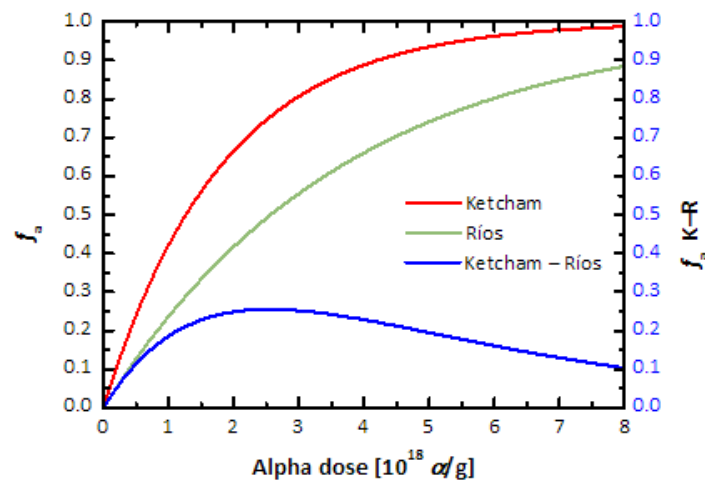


Figure 1: Plot comparing amorphous fractions from X-ray diffraction measurements (Ríos et al., 2000; green) and the geometrical damage connectivity model built by Ketcham et al. (2013; red). The blue curve shows the difference as a function of the recoil events per gram.

3.5. Inelastic neutron scattering and first-principles calculations

Vibrational spectroscopy probes the transitions between vibrational energy levels. The most widespread analytical methods are Raman and infrared absorption spectroscopy, which are based on the inelastic scattering and resonant absorption, respectively, of photons of appropriate energies. The interactions are subject to symmetry-governed selection rules as well as the $k = 0$ wavevector selection rule in crystals of sufficient size. These methods are relatively cheap, readily accessible with widely available expertise, and can be coupled to optical microscopes to study small samples. In contrast, inelastic neutron scattering (INS) also provides a probe of vibrational energy

levels via inelastic scattering of (epi)thermal neutrons (a few to a few hundred meV and beyond). An INS spectrum is not dissimilar to IR and Raman spectra, though selection rules are different. Neutrons have small wavelengths and a small mass while their interaction with matter is fundamentally different (nuclear instead of electronic), and it is possible to measure both momentum and energy transfer from scattered neutrons to the target. Specifically, it is possible to acquire phonon dispersion (energy transfer vs. wavevector) curves of optical and acoustic phonon branches in the entire Brillouin zone of a crystal. This is helpful in the study of vibrational properties not easily accessible through optical methods, for instance phonon confinement effects. The disadvantages of the method include that the interaction with neutrons is very weak, therefore large samples are necessary, and that neutron sources are enormous, highly complex apparatuses of which only a few exist worldwide. Specifically, for the study of higher energy transfers (approximately >50 meV), a spallation neutron source is necessary, of which only two exist in Europe (Swiss Spallation Neutron Source, SINQ, and ISIS Neutron and Muon Source in the UK). The INS literature for zircon is very sparse, only a single source of an experimental determination of phonon dispersion curves is known, and even that one is lacking higher-energy optical modes (Chaplot et al., 2006, and references therein).

Inelastic neutron scattering experiments are generally accompanied by first-principles modelling to help interpret and verify experimental data. Quantum mechanical calculations can be used to compute the electronic structure of many-body systems using density functional theory (DFT). As a complete solution of quantum mechanical equations describing complex systems is impossible, DFT makes calculations feasible based on an approach where electronic properties are determined through functionals of the electron density. DFT modelling makes possible to calculate vibrational modes, phonon frequencies and dispersion relations. The numerical simulation of larger unit cells (the 12 atoms in the primitive unit cell of zircon accounts as large) is computationally intensive, but at the appropriate theoretical level and with a correct choice of pseudopotentials the calculated properties can prove to be very close to experimental data. Thus, a DFT calculation of phonon dispersion relations in zircon was held to be highly desirable.

4. Results

The results presented here include a short summary of the progress made during the project, including theoretical and practical knowledge acquired, or reconsidered, through all the effort put into the research activity.

4.1. Electron-beam annealing of thick samples

The findings of the electron-induced annealing were published as a journal article (Vácz & Nasdala, 2017); they will be summarised here shortly. The motivation for the study included a systematic, in-depth exploration of the electron beam-induced alteration effect of zircon, as a phenomenon inevitable in EPMA analysis. An attempt was also made to interpret the observed effect, through measurable changes in Raman parameters, in terms of the structural recovery of zircon.

The most important outcome of this study was to establish that it is the electron dose (or fluence) that determines the extent of the annealing process. The electron dose was approximated by the product of the beam current and the irradiation time because of technical limitations in quantification. In short, very small electron doses are insufficient to cause observable changes, therefore, scanning electron imaging even with high beam currents is safe until the scanning is not overly extended in time (such as in cathodoluminescence imaging). The magnitude of the change in Raman parameters is larger when initial zircon materials are more self-irradiation damaged. In addition, the electron-induced annealing effect (the rate of change) was observed to level off at

increased electron doses, suggesting that the annealing effect is kinetically limited in the sense that not all damage could be healed (Fig. 2).

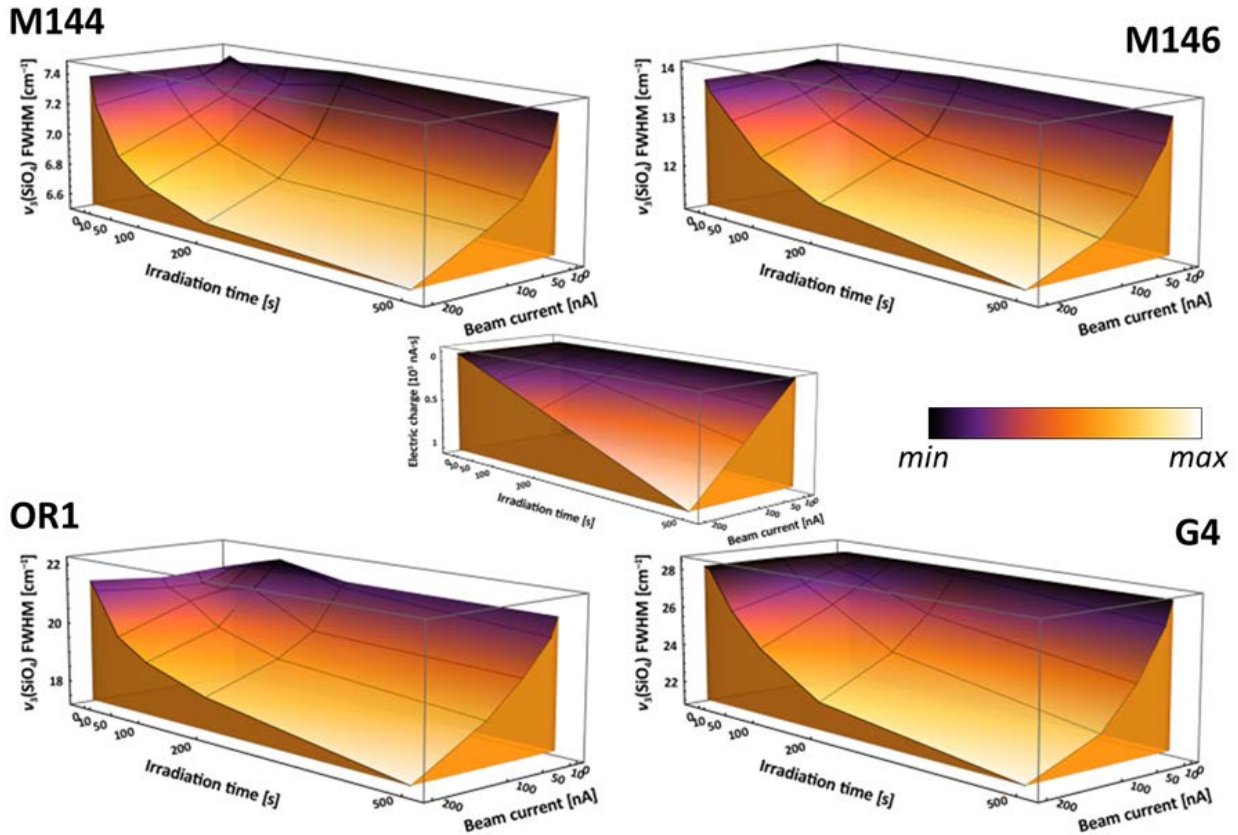


Figure 2: Surface plots of Raman $\nu_3(\text{SiO}_4)$ FWHM data from electron-beam annealed bulk zircon samples. The smaller surface plot in the centre shows the electron dose (as a product of time and current). The total change is proportional to initial damage levels (indicated by the back edges), similar doses have similar annealing effects, and the rate of change levels off at increasing electron doses.

The changes observable through Raman scattering were attributed to defect reactions, induced by low-energy electrons, in the non-amorphised volume of radiation-damaged zircon. The rate of change in Raman FWHMs seemed to slow down at higher electron doses, possibly signalling a limitation of the annealing effect. It was possible to rule out the role of heating (thermal annealing) of bulk zircon by the electron beam (the recovery depended on dose at any beam current). Note that bulk is used here in the sense that the sample volume is much larger than the interaction volume with the electron beam. The formula for a previously published, empirical damage accumulation curve relating $\nu_3(\text{SiO}_4)$ FWHM and alpha dose was also improved, to compare estimates of typical undamaged crystal sizes (Ketcham et al., 2013) to Raman FWHMs as a function of alpha dose (Fig. 3). Using the damage connectivity model of Ketcham and co-authors, a tentative visualisation of the recovery of scattering translational domains was also produced (Fig. 3). The potential practical aspects of the results were also evaluated: recommendations were made for zircon analytical work and the potential of the method to create waveguides in naturally damaged or ion-irradiated zircon was highlighted.

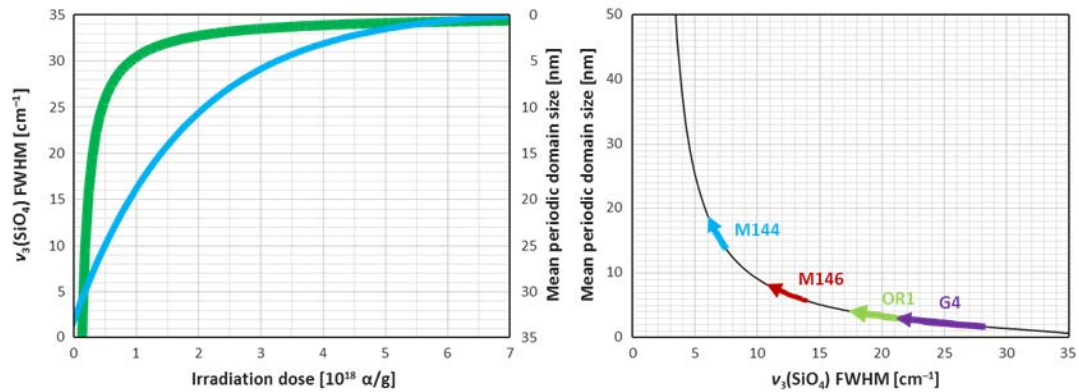


Figure 3 Left: a comparison of the evolution of the zircon Raman $\nu_3(\text{SiO}_4)$ FWHM trend as a function of alpha dose (best fit to empirical data) and the undamaged crystalline domain sizes from a recoil connectivity model (Ketcham et al., 2013). Right: the solid curve is constructed from the data in the figure on the left, and the extent of maximum recovery (at 200 nA, 500 s irradiation) for each electron-annealed sample is shown.

4.2. Ion irradiation of samples

Sample preparation

Sample preparation for ion irradiations was a major task in the project. The choice of FIB-SEM preparation of lamellae was an obvious choice in the sense that the method is routinely used for the preparation of electron-transparent foils for transmission electron microscopy (TEM) work. The preparation of samples for this project is a modification of the TEM lamella preparation procedure. The thickness was aimed to be 1.5 μm instead of electron transparency (<100 nm), to be a good match for subsequent optical analysis interaction volumes. The lamellae were cut in the FIB-SEM laboratory of the Faculty of Sciences, Eötvös Loránd University, intermittently through an extended time period, during which, at one point, the bulk crystal was used at a certain rotation angle to cut further lamellae, without consulting me. The rotation was recognisable in band intensity ratios in Raman analyses, but caused probably no major problem in irradiations as well as their evaluation as neither position, nor FWHM does not change with the rotation of the scattering tensor, while ion channelling in irradiations is not a major issue in these thinned samples.

He-ion irradiation

The irradiation of FIB-prepared lamellae with He^{2+} ions to imitate alpha particle-induced damage saw significant delay due to experimental concerns. The very narrow stopping range of mono-energetic ions produces damage in a small volume which is problematic because of analytical (due to the diffraction-limited sampling volume of optical microscopy methods) and mechanical issues (the damage-induced swelling creates a poorly measurable strain field around the stopping range; see Nasdala et al., 2010). The preparation of 1.5 μm thick lamellae was introduced to circumvent the strain problematics but leave enough material for safer handling, optical sampling etc. (Chanmuang et al., 2016).

Following an earlier publication (Csato et al., 2015), an ion-beam energy filter was custom prepared that created a spread in the He ion kinetic energies. The pre-calculated energy spread formed a “plateau” in knock-on energy transfer, in which the lamellae were placed. The result was that the entire volume of the lamellae were damaged evenly, avoiding strain problems. To create the light ion induced damage within the FIB-prepared lamella, the ions had to be slowed down, as the stopping range of 8.8 MeV He is ca. 32 μm in pristine zircon. To control the deceleration in the electronic interaction regime precisely, a $\sim 18.5 \mu\text{m}$ thick, commercially available copper foil was

placed in the ion path. The procedure was published in a conference paper (Nasdala et al., 2017) and in detail in a later article (Nasdala et al., 2019). In addition, custom-made filter and sample holders were also designed at the Institute for Mineralogy and Crystallography, University of Vienna, that accommodated up to three samples and were also designed to suppress nuclear activation problems (Nasdala et al., 2019). Altogether, due to the enormous complexity of sample preparation as well as a delay in the availability of a substrate for the production of the energy filter, the light-ion irradiations were finally accomplished at the end of the second project year.

The meticulously prepared He-irradiation experiment produced a sample set that showed a monotonous increase of radiation effects in spectroscopic parameters (Fig. 4; Váczi, 2018). This sample set was planned to be the subject of electron-beam annealing.

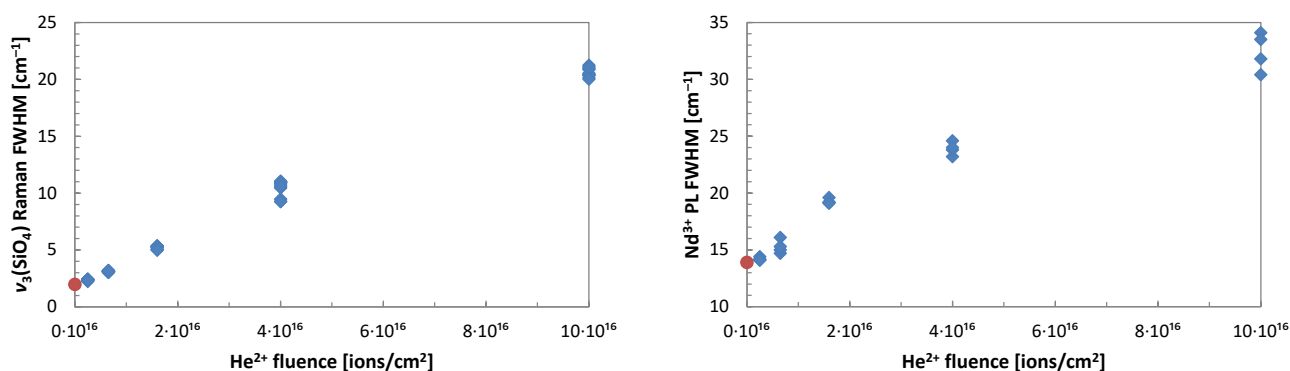


Figure 4: Plot of band widths measured on He-irradiated lamellae as a function of He ion fluence. For reference, the average of FWHMs from unirradiated lamellae is included (orange dot). Left: $v_3(\text{SiO}_4)$ Raman band; right: Nd^{3+} PL emission band (${}^4F_{3/2} \rightarrow {}^4I_{9/2}$) at ca. 11360 cm^{-1} .

Au-ion irradiation

Heavy-ion irradiation was finally not performed in the time frame of the project. There were numerous reasons; in the first place, due to a miscommunication issue, for a long time it was unclear that the heavy-ion irradiations were not part of the planned irradiation session at the Helmholtz-Zentrum Dresden-Rossendorf. The application for beamtime was handled by the cooperation partner at the University of Vienna and the information was regrettably lost (which, in turn, resulted in a personal communication problem between partners). A study, however, was published during the course of this project, reporting on the heavy-ion irradiation and the Raman and PL analysis of FIB-milled zircon foils, which is basically identical to this project's sample preparation steps (Nasdala et al. 2018), but without the electron annealing part and subsequent analysis. It would have been of no practical benefit to replicate the findings of this study, since, in the lack of a suitable electron-beam annealing method, no additional experiments could be added and no new knowledge could be established.

4.3. Electron-beam annealing of thinned samples

The electron-irradiation of FIB-cut lamellae followed the spectroscopic characterisation of ion-irradiated samples. Based on conclusions drawn from the bulk irradiation study (Váczi & Nasdala, 2017), the annealing experiments were planned with a high electron fluence, such as the highest electron fluences (doses) in the bulk study. The SEM instrument was selected based on availability. As the two main limiting factors were the instrument time and potential sample/beam drift during irradiation (while no imaging control is available), a high, 200 nA beam current was applied and a set of He-irradiated samples was annealed in a single session. Tests in the bulk study clearly

discouraged the application of a conductive coat, as it is not removable from samples of this size while it may introduce artefacts (surface enhanced scattering in case of gold, or strong, broad Raman background in case of carbon) that cannot be treated well during data reduction. Subsequent analysis of the changes in the zircon $\nu_3(\text{SiO}_4)$ Raman parameters compared to post-He, pre-electron irradiation values revealed that the annealing effect was most extensive in the intended irradiation spots but, to some degree, was observable in the entire lamellae (Fig. 5). In addition, unusual Raman parameters (especially a downshift of the $\nu_3(\text{SiO}_4)$ band position at the edge of the lamella; Fig. 5) suggest an additional artefact, possibly strain that developed in the lamella. The effects of the electron-beam irradiation were utterly unexpected, and prevented the correct quantitative evaluation of the annealing effect because the electron fluxes became unpredictable and strain effects possibly influenced the measurable Raman values.

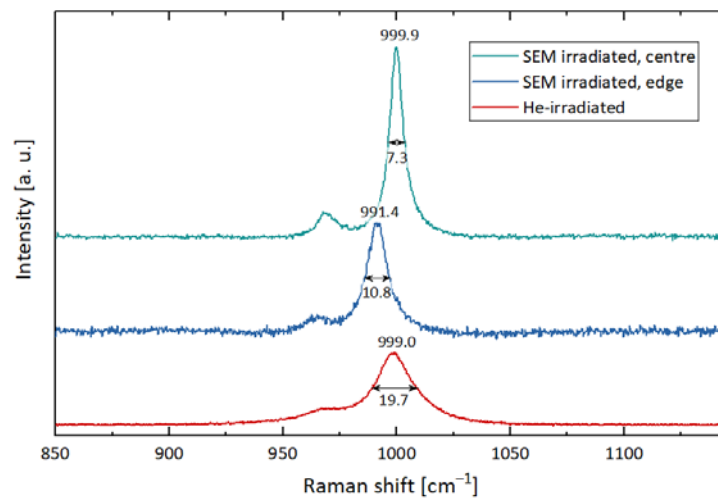


Figure 5: Raman spectra of a FIB-cut lamella, irradiated with an ion fluence of $1.0 \cdot 10^{17} \text{ He/cm}^2$. Fitted $\nu_3(\text{SiO}_4)$ band positions and FWHMs are marked on each spectrum. Red curve: before electron irradiation; blue curves: after electron irradiation in the SEM (middle: edge of lamella; top: centre of lamella).

Consequently, another round of electron irradiation was planned, using a different system, on the available backup sample set. A cryo-SEM, that is, an SEM with a deep-cooled (by liquid N_2 , at 77 K) sample stage appeared to be practically unavailable. Furthermore, it appears intuitively that a cooled sample stage may be limited to draw the generated heat away, at a sufficient rate, from the irradiation spots in the lamellae through the bottleneck presented by the deposited small platinum connection between the lamellae and the lift-out grids. The modelling of heat flow or an estimation of the heat rise or was not feasible due to the size of the task presented by the complicated geometry.

An instrument capable of less aggressive electron irradiation was identified. The RAITH 150 e-beam writer is a scanning electron microscope-type instrument primarily aimed at high-resolution electron lithography. Its specialised purpose means that it is equipped with capabilities not found on regular SEM's or EPMA's: in addition to usual beam delivery controls, at defined intervals it is able to pause the beam, relocate exactly the same spot on the sample to avoid drift, and do this for an extended time. It was set up to deliver a stationary beam at reduced beam current and some defocus to decrease the electron flux density, increase the irradiation volume etc. The parameters were partly chosen to be a best compromise in available instrument time and optimum settings for the analytical goal (20 kV, 1.228 nA, 60 μm limiting aperture, defocus to approx. 500 nm spot size

as measured using intensity fall-off on the Faraday cup). Although the beam current could have been decreased even more, the net beam dwell time was 22.4 hours, not including the intermittent imaging and relocation steps, in one such electron irradiation experiment with the above settings. The e-beam writer was tested on one helium-irradiated lamella ($1 \cdot 10^{17}$ He/cm²) of the backup set to establish the viability of the changed electron irradiation parameters.

The data (smaller band widths) from the subsequent Raman analysis of the sample irradiated using the e-beam writer also showed, albeit to a lesser degree, that partial annealing occurred again within the entire lamella. The annealing effect may be attributed to the heating effect of the electron beam current, elevating the temperature of the lamellae possibly to excessive levels. The major difference to bulk sample irradiation experiments is interpreted such that the part of the electron energy that turned into heat was not able to escape through conductive transfer without the bulk crystal (and partly the gold coat) acting as a heat sink. This happened despite the fact that the lamella thickness was actually less than the electron penetration depth (see electron Monte Carlo simulation in Vácz & Nasdala 2017); however, the majority of electron stopping occurred in the lamellae. Another possible explanation for the spatially expanded annealing of the lamellae could be a poorly controlled beam size at the sample surface. The lack of a conductive coat caused the build-up of electric charge on the samples that may have resulted on the skirting of the beam. If so, an area (volume) was annealed that was larger than it could be expected from the realistic beam geometry without charging effects. The conclusion in Vácz & Nasdala (2017) that even fairly electron energies ($\ll 20$ keV) may be sufficient to cause defect reactions is possibly relevant here.

The annealing effect is experimentally irreversible, therefore the rest of the sample set was not electron irradiated, in hope of a superior solution. In the time frame of the project, however, such a solution was not found.

4.4. Photoluminescence

Photoluminescence analysis was included in the project in order to have a method that provides contrasting information, when compared to Raman spectroscopy, about the real structure of zircon. Though PL spectra were duly recorded (an example is shown in Fig. 4), the perception of the data and their information content has undergone a profound transformation. This is discussed here in the following subsection.

Luminescence emission from solids is often regarded as a local probe of crystal fields, and their distortions, around REE impurities in zircon. While this specific picture is not challenged here, the issues regarding the PL signals in the radiation damage trend (e.g. Lenz & Nasdala, 2015) and the proportion of the crystal field to the experimental sampling volume had to be reconsidered.

The crystal field splitting in the electron energy levels of a $4f$ luminescence centre gives rise to a number of sharp emission bands (up to 10 in the case of Nd³⁺). The luminescence emission (in the following discussion I will keep mentioning PL only) band widths in highly ordered crystal hosts are typically of a few wavenumbers. As a kind of alternative measure, it was described that PL bands show a progressive band broadening and loss of emission intensity as a function of the calculated alpha dose in zircon (as well as in other materials not covered here), up to an almost featureless, feeble signal from radiation-amorphised zircon (see Lenz & Nasdala, 2015; Lenz et al., 2019). It was demonstrated that either PL band widths (Lenz & Nasdala, 2015) or envelope curves covering multiple sub-bands (Lenz et al., 2019) were able to produce quantitative damage accumulation trends, albeit with some analytical difficulties mainly involving band overlap and background treatment. However, an in-depth assessment suggested that the PL vs. dose curves do not offer significant advantages in their sensitivity to damage; in fact, they seem to be the little brother of Raman damage accumulation curves, with more analytical uncertainty (see also Ende et al., 2021.)

The PL emission (and, as a matter of fact, Raman) signal shows heterogeneous broadening at any damage level other than zero. The emission bands may be broadened per se by decreased lifetimes when defects and lattice (crystal field) distortions are introduced. However, a multitude of emission centres are sampled by any given luminescence technique if REE centres are present even in the low range of natural abundances. The following quick estimation may aid the discussion. The volume of the tetragonal unit cell of zircon is approx. 260 \AA^3 , in which there are four $4a$ ($\text{Zr}^{[8]}$) sites where REE substitutions may take place. The so-called micro-spectroscopic techniques sample at least a few μm^3 ; if this is taken somewhat arbitrarily at $2.5 \mu\text{m}^3$, a unit conversion gives us approx. 10^9 Zr sites per sampling volume. A very low REE³⁺ ion concentration of e.g. 10 ppm by abundance (REE ion/Zr site) gives about 10^4 emission centres per sampling volume. From a mineralogical or geochemical point of view, this volume counts indeed as micro-sampling, but still a significant number of emission centres are averaged. Thus, if there is a distribution of defects or disorder, we are measuring heterogeneous broadening in PL spectroscopy. Indeed, both the fitted band shapes (Lenz & Nasdala, 2015) and the broadened PL emission envelopes (Lenz et al., 2019) are not connected to any known distribution of irregularity (defects, strain etc., i.e., an actual physical quantity) in the sampled population of crystal fields, but they are evaluated through the proxy of independently determined, calculated alpha doses. Note, however, that even the assumption of heterogeneous broadening is not fully compatible with all details: the presence of defects should produce mixed signals in PL bands (e.g. a sharp band shape from regular crystal fields superimposed with broadened bands from coordinations affected by defects to varying degrees). Though broadening of PL bands is correlated with increasing radiation damage in zircon, prominent mixed-signal effects are not observable (and would be extremely difficult to handle correctly). This observation (Vácz, 2018) questions the validity of PL emission being only a local probe of coordination spheres.

The arguments outlined above have shifted significantly the understanding of PL emission spectroscopy of zircon damage and annealing. First, PL micro-spectroscopy is nonetheless a bulk method (in the sense mentioned earlier): the volume it averages is much larger than the physical source of the signal(s) unless the density of colour centres is on the order of 1 ppb by volume. Second, the proxy curve of PL band widths (or envelopes) vs. calculated alpha dose allows only a comparison of any measurement to the natural damage accumulation trend. Things only get more complicated in the case of annealing, since annealing is not a direct reversal of damage accumulation (e.g., Geisler et al., 2001; Ende et al., 2021). The recovery of crystal fields around the Zr sites is not yet understood from bulk data from long-range effects such as X-ray diffraction (e.g. Ende et al., 2021) but computer simulation may bring progress in this subject (see e.g. Yang et al. 2018).

In summary, PL data had been assumed to provide information on short-range ordering, but new data and new insights transformed their perception to a point where they are seen as insufficient to explain the real structure of the interaction volume. To date, there is no universal atomistic or statistical model of damage accumulation, and the heterogeneously broadened PL emission bands are not understood in adequate depth to give actual insight to the influence of nearest-neighbour effects (bond lengths, vacancies and interstitials, distortions etc.). The improved understanding of the phenomenon and the analytical method, unfortunately, led to a disconcerting lack of new knowledge in this part of the project.

4.5. Computer simulations and INS

The geometric modelling of damage distribution was started as a 2D approximation while options were being searched for creating a comprehensive 3D model. The 2D model was based on pixels,

and the number of pixels was scaled up to diminish pixelation artefacts. Pixel clusters (e.g., 5×5) could take the state of being “undamaged” and “damaged” in a simulation box to model alpha recoil damage clusters in a crystal. After adding a number (100–100 000) of randomly distributed “damage” clusters to the simulation box, the distribution of the sizes of undisturbed areas was evaluated. The main aim of this modelling was to find the size of undisturbed volumes (areas in the 2D model) because these dimensions are thought to be of relevance to phonon mean free paths (and, hence, phonon lifetimes and Raman band widths) in real samples. Straight lines of random origin and direction were used to probe the size distribution of undisturbed areas. Line lengths up to their first intersection with the simulation box edges or a “damaged” pixel cluster were recorded. Note that this implementation produces length distributions that are biased probably towards shorter intercept lengths because the random lines were not projected in both directions; however, the box dimensions (lengths of the edge and the diagonal) were apparent on the length histograms.

The model proved to be highly educative. Evaluating 250000 lines in a large, 32000×32000 pixel simulation box (i.e., over 10^9 pixels), the influence of “defects” was already discernible on the length distribution histogram after adding 1000 randomly placed, 5×5 pixel “damaged” clusters. This corresponds to an extremely low “damaged” or “amorphous” fraction of $2.4 \cdot 10^{-5}$ (Fig. 6). Adding more “defects” enhanced the shift to shorter intercept lengths, though a measure for quantification better than the distribution peak not found. The effect of cluster size was also tested by approximately doubling the “defect” cluster sizes, from 5×5 to 7×7 pixels, and comparing the effect on length distribution to doubling the number of 5×5 “defects”. At the same “damaged” fraction of $4.8 \cdot 10^{-4}$, the intercept lengths were limited more effectively by the larger number of defects than by the larger cluster size (Fig. 6). This observation can be translated to the statement that the connectivity model of Ketcham et al. (2013) overestimated the undamaged domain sizes at any given damage density (though this does not necessarily translates to an earlier onset of the massive connectivity of defects).

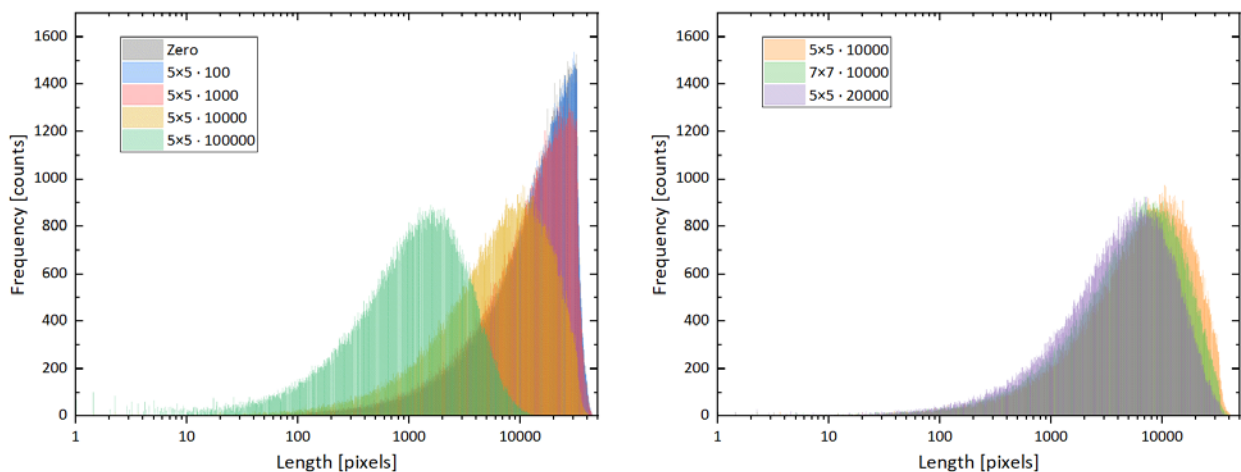


Figure 6: Intercept length distributions from a 2D modelling of randomly distributed pixel clusters in a 32000×32000 simulation box. Left: the effect of the number of 5×5 pixel clusters. The difference between zero and 100 clusters is not discernible. Right: The effect of cluster density vs. cluster size: the green and violet distributions represent approximately the same ratio of total cluster area to the area of the simulation box. Twice as many pixel clusters are more effective than the same number of clusters with double area in limiting intercept lengths.

It was estimated that if the evaluation was made using discs or another 2D shapes in this model, the decrease of “undamaged” sizes would be much more pronounced with the increase of the

“damage fraction”. Though this model’s shortcomings were evident (2D space, evaluation using lines), it provides a strong intuitive indication of how quickly the accumulation of defects or defect clusters may limit the sizes of undisturbed volumes in self-irradiated materials. This is linked directly to the issue of translational phenomena, such as the propagation of phonons. Indeed, in line with the conclusions of the Ketcham et al. (2013) study, the decrease of volumes with undisturbed translational symmetry appears to evolve surprisingly quickly with increasing defect densities. In addition, even this rudimentary model provided new insight into the better understanding of the defect-free dimensions. The correct size of the individual recoil clusters are crucial when the amorphous fraction is used as the order parameter: wrong recoil sizes apparently give incorrect dimensions for defect-free regions.

The 2D model offered a lot of direct and indirect insight. In addition to seeing the evolution of undamaged sizes, it became clear that the move to a geometric 3D model of recoil cluster accumulation would constitute a very large undertaking in terms of programming as well as computing power. An appropriate solution has to move from the limitation caused by pixels (voxels) to a vector-based model, while still being large enough, and/or employ specific boundary conditions, to suppress the effect of the simulation box boundaries. In addition, the evaluation of a very large number of recoil clusters is needed to account for a reasonable degree of partial amorphisation because of the large simulation box as well as for statistical reasons. Another conclusion is that the performance of a high-level computing language environment such as MATLAB is expected to be impractical (i.e., too slow) due to the complexity of, and the large number of calculations necessary in, the assessment of cluster spacing (undisturbed volume size distribution). A fully custom-made code, possibly employing GPU acceleration seems to be more suitable for the 3D model. Arrangements are still under way to come to an agreement with a cooperation partner with resources to allocate to this problem (time for writing the code and access to infrastructure), but unfortunately the start of 3D modelling cannot be reported.

A DFT calculation of the phonon dynamics of zircon, without INS measurements, has been published recently (Sheremetyeva et al, 2018). A single but very important aspect of these calculations is that the dispersion curve for the $\nu_3(\text{SiO}_4)$ B_{1g} phonon mode shows decreasing frequencies for increasing k -vectors. This result is highly interesting in view of the damage-induced downshift of this mode frequency (e.g. Nasdala et al., 2004) because the shift in Raman frequencies due to phonon confinement (a k -vector shift due to space- or time-limited phonon propagation) typically follows the phonon dispersion trends (see e.g. Osswald et al., 2009). Combined with the estimation of undamaged domain sizes from geometric modelling, the phonon dispersion curves could provide interesting new results or ideas for Raman analysis. Since the DFT calculations included strain effects (Sheremetyeva et al, 2018), they could be used possibly to make a nanoscale strain analysis, and compare that to possible phonon confinement effects. However, this is beyond the scope of this project.

The experimental study of higher-energy phonon dispersion curves was attempted, first by consulting experts and users of inelastic neutron scattering, including scientific staff at the Budapest Neutron Centre. It turned out that the >100 meV energy transfer necessary to “map” the focus of the Raman transition here ($\nu_3(\text{SiO}_4)$ mode) is not achievable in nuclear reactor neutron sources (which is also why the INS plots in Chaplot et al., 2006 lack data above 50 meV). Despite an actual agreement on sourcing an adequate sample, as well as continued efforts to organise an INS measurement at a spallation neutron source, I was not able to compile and submit a proposal for INS infrastructure access.

5. Benefits beyond results and lessons learnt

The aim of the project was to improve the understanding of the real structure of radiation-damaged zircon. A lot of “soft” skills, insight and experiences were gained, bringing many benefits to the PI beyond actual scientific outcome. The systematic study of electron-annealed bulk zircon, performed in the frame of the project, revealed hints to annealing kinetics driven by electron-induced defect reactions and practical wisdom regarding electron microprobe analytical practice. A lot of experience was gained from using a large-scale facility and from the close look at the amount of planning necessary prior to actual experiments. Access to several different types of electron-beam apparatuses was organised, analytical skills of using optical spectroscopic instruments were improved. The addition of modelling to physical experiments provided results that helped the assessment of published data, identifying their shortcomings and making important predictions.

The ion-irradiation and subsequent spectroscopic analysis of zircon was a very complex undertaking, in which not everything progressed according to plans. The planned analytical tasks were not completed according to the original plans, partly hindered by a management setback, as well as by analytical difficulties (e.g. a lack of an appropriate electron-annealing method). As a consequence, a change in project goals was requested. Some of the planned tasks (Au⁺ irradiation of FIB foils and the subsequently proposed of DFT analysis) were published by other researchers; nevertheless, useful knowledge came from these articles.

The limitations in the successful completion of planned tasks can be traced back to a multitude of reasons, partly to changes in the professional (job change to outside earth sciences and participating in multiple research projects) and the personal life of the PI (family formation and an inevitable shift in priorities). It was also possible to establish that there is room to improve on managerial skills that involve personal contact with other researchers, for instance to access analysis methods outside the PI's own expertise. The course of the project also revealed some shortcomings in the planning, partly traceable to a biased understanding of methods (as in the case of photoluminescence spectroscopy or the electron irradiation of small dielectric samples), and partly to the finite availability of personal resources besides a full time job of teaching or doing research in another field. In addition, an important lesson learnt is that in the case of multiple options for experiments being available, it is always wiser to pick the one where more expertise is given over the one of local availability, avoiding choices biased by compliance with imagined expectations, real or not.

The complex assessment of obtained experimental and theoretical data provided a greatly improved understanding of phenomena and processes regarding the accumulation and annealing of radiation damage, including a reassessment of what “bulk” means in relation to information content; an improved view of Raman scattering and PL emission in solids; an insight into phonon dispersion relations and their calculation; and the importance of numerical methods in material analysis.

6. References

- Chanmuang, C., Habler, G., Lenz, C., Nasdala, L. & Váczi, T. (2016): Quantification of radiation effects in zircon: Focused-ion beam preparation of thin lamellae for ion-irradiation experiments. Book of Abstracts. EMC2016 2nd European Mineralogical Conference, 2016, no. 15–15
- Chaplot, S.L., Pintschovius, L. & Mittal, R. (2006): Phonon dispersion relation measurements on zircon, ZrSiO₄. *Phys. B*, **385–386**: 150–152
- Csato, C., Krippendorf, F., Akhmadaliev, S., von Borany, J., Han, W., Siefke, T., Zowalla, A., Rüb, M. (2015): Energy filter for tailoring depth profiles in semiconductor doping application. *Nucl. Instr. Meth. Phys. Res. B*, **365**: 182–186
- Ende, M., Chanmuang N., C., Reiners, P.W., Zamyatin, D.A. & Gain, S.E.M., Wirth, R. & Nasdala, L. (2021): Dry annealing of radiation-damaged zircon: Single-crystal X-ray and Raman spectroscopy study. *Lithos*, **406–407**: 106523
- Farnan I. & Salje, E.K.H. (2001): Degree and nature of radiation damage in zircon observed by ²⁹Si nuclear magnetic resonance. *J. Appl. Phys.*, **89**: 2084–2090
- Finch, R.J. & Hanchar, J.M. (2003): Structure and Chemistry of Zircon and Zircon-Group Minerals. In: Hanchar, J.M., Hoskin, P.W.O. (eds): *Zircon /Rev. Mineral. Geochem.*, 53/. Mineral. Soc. Am., Washington DC, 1–25
- Geisler, T., Pidgeon, R.T., van Bronswijk, W. & Pleyzier, R. (2001): Kinetics of thermal recovery and recrystallization of partially metamict zircon: a Raman spectroscopic study. *Eur. J. Mineral.*, **13**: 1163–1176
- Ketcham, R.A., Guenther, W.R. & Reiners, P.W. (2013): Geometric analysis of radiation damage connectivity in zircon, and its implications for helium diffusion. *Am. Mineral.*, **98**: 350–360
- Lenz, C. & Nasdala, L. (2015): A photoluminescence study of REE³⁺ emissions in radiation-damaged zircon, *Am. Mineral.*, **100**: 1123–1133
- Lenz, C., Thorogood, G., Aughterson, R., Ionescu, M., Gregg, D.J., Davis, J. & Lumpkin, G.R. (2019): The quantification of radiation damage in orthophosphates using confocal μ -luminescence spectroscopy of Nd³⁺. *Front. Chem.*, **7**: 13
- Osswald, S., Mochalin, V. N., Havel, M., Yushin, G. & Gogotsi Y. (2009): Phonon confinement effects in the Raman spectrum of nanodiamond. *Phys. Rev. B*, **80**: 075419
- Nasdala, L., Zhang, M., Kempe, U., Panczer, G., Gaft, M., Andrut, M. & Plötze, M. (2003): Spectroscopic methods applied to zircon. In: Hanchar, J.M., Hoskin, P.W.O. (eds): *Zircon /Rev. Mineral. Geochem.*, 53/. Mineral. Soc. Am., Washington DC, 427–467
- Nasdala, L., Reiners, P.W., Garver, J.I., Kennedy, A.K., Stern, R.A., Balan, E. & Wirth, R. (2004): Incomplete retention of radiation damage in zircon from Sri Lanka. *Am. Mineral.*, **89**: 219–231
- Nasdala, L.; Grötzschel, R.; Probst, S.; Bleisteiner, B. (2010): Irradiation damage in monazite-(Ce): An example to establish the limits of Raman confocality and depth resolution. *Can. Mineral.*, **48**: 351–359
- Nasdala, L., Grambole, D., Götze, J., Kempe, U., Váczi, T. (2011): Helium irradiation study on zircon. *Contrib. Mineral. Petrol.*, **161**: 777–789
- Nasdala, L., Akhmadaliev, S., Chanmuang, C., Csato, C., Rosen, T., Rüb, M., Váczi, T., Wagner, A., Zowalla, A. (2017): A promising tool for the investigation of alpha-particle damage in accessory minerals: ⁴He irradiation using a fabricated, Si-based energy filter. Book of Abstracts, CAM-2017 Conference on Accessory Minerals, 83–84
- Nasdala, L., Akhmadaliev, S., Artac, A., Habler, G. & Lenz, C. (2018): Irradiation effects in monazite-(Ce) and zircon: Raman and photoluminescence study of Au-irradiated FIB foils. *Phys. Chem. Minerals*, **45**: 855–871

- Nasdala, L., Akhmadaliev, S., Chanmuang, C., Zowalla, A., Csato, C., Rüb, M. (2019): ^4He irradiation of zircon, ZrSiO_4 , using a micro-patterned, Si-based energy filter. *Nucl. Instr. Methods Phys. Res. B*, **443**: 38–42
- Ríos, S., Salje, E.K.H., Zhang, M. & Ewing, R.C. (2000): Amorphization in zircon: evidence for direct impact damage. *J. Phys.: Condens. Matter*, **12**: 2401–2412
- Salje, E.K.H., Chrosch, J. & Ewing, R.C. (1999): Is “metamictization” of zircon a phase transition? *Am. Mineral.*, **84**: 1107–1116
- Sheremetyeva, N., Cherniak, D.J., Watson, E.B. & Meunier, V. (2018): Effect of pressure on the Raman-active modes of zircon: A first-principles study. *Phys. Chem. Minerals*, **45**: 173–184
- Smye, K.M., Brigden, C., Vance, E.R. & Farnan, I. (2014): Quantification of α -particle radiation damage in zircon. *Am. Mineral.*, **99**: 2095–2104
- Trachenko, K.O., Dove, M.T. & Salje, E.K.H. (2001): Atomistic modelling of radiation damage in zircon. *J. Phys.: Condens. Matter*, **13**: 1947–1959
- Váczi, T. (2014): A new, simple approximation for the deconvolution of instrumental broadening in spectroscopic band profiles. *Appl. Spectrosc.*, **68**: 1274–1278
- Váczi, T. (2016): Are there point defects in the crystalline portion of self-irradiated minerals? Book of Abstracts. EMC2016 2nd European Mineralogical Conference, 2016, 15–16
- Váczi, T. (2018): Spectral changes caused by particle irradiations in zircon. Abstract Book, GeoRaman 2018 Conference (missing page number)
- Váczi, T. & Nasdala, L. (2016): Phonon confinement in radiation-damaged zircon. Abstract Volume, XII International Conference GeoRAMAN-2016, 61
- Váczi, T. & Nasdala, L. (2017): Electron-beam-induced annealing of natural zircon: a Raman spectroscopic study. *Phys. Chem. Minerals*, **44**: 389–401
- Yang, X.-Y., Wang, S., Lu, Y., Bi, P., Zhang, P., Hussain, Sh., Yi, Y. & Duan, T. (2018): Structures and energetics of point defects with charge states in zircon: A first-principles study. *J. Alloys Comp.*, **759**: 60–69
- Zeug, M., Nasdala, L., Wanthanachaisaeng, B., Balmer, W.A., Corfu, F. & Wildner, M. (2018): Blue zircon from Ratanakiri, Cambodia. *J. Gemmol.*, **36**: 112–132

Talks related to the project, without a published abstract:

- Váczi, T.: Transzlációk doménméretek sugárkárosodott cirkonban (Translational domain sizes in radiation-damaged zircon). Téli Ásványtudományi Iskola, 2016, Balatonfüred.
- Váczi, T.: Raman-spektroszkópia a magmaképződéstől a bioszféráig: amit máshogy nem tud(hat)tunk volna meg (From magma formation to the biosphere: things we could not learn without Raman spectroscopy). Téli Ásványtudományi Iskola, 2017, Veszprém.
- Váczi, T. & Nasdala, L.: The effects of helium irradiation on the optical spectroscopic properties of zircon. Téli Ásványtudományi Iskola, 2018, Veszprém